Research Square

Preprints are preliminary reports that have not undergone peer review.
They should not be considered conclusive, used to inform clinical practice,
or referenced by the media as validated information.

Non-monotonic Plasmon-Induced Transparency in Asymmetric Terahertz Metasurfaces Integrated with Vanadium Dioxide

Tae-Han Kim
Hankuk University of Foreign Studies
Ji Hun Seo
Hankuk University of Foreign Studies
Ye Jin In
Hankuk University of Foreign Studies
Da Gyeong Lee
Hankuk University of Foreign Studies
Bo Wha Lee
hsolab2022@gmail.com
Hankuk University of Foreign Studies

Research Article

Keywords: non-monotonic plasmon-induced transparency, asymmetric terahertz metasurface, vanadium dioxide, insulator-to-metal transition, coupled-mode theory

Posted Date: September 10th, 2026

DOI: https://doi.org/10.21203/rs.3.rs-10894789/v1

License: This work is licensed under a Creative Commons Attribution 4.0 International License.
Read Full License

Additional Declarations: No competing interests reported.

Non-monotonic Plasmon-Induced Transparency in Asymmetric Terahertz Metasurfaces Integrated with Vanadium Dioxide

Tae-Han Kim[1], Ji Hun Seo[1], Ye Jin In[1], Da Gyeong Lee[1], and Bo Wha Lee[1*]

[1]*Department of Physics and Oxide Research Center,*

Hankuk University of Foreign Studies, Yongin 17035, South Korea

[*] Corresponding author: hsolab2022@gmail.com

Abstract

Non-monotonic plasmon-induced transparency (PIT) is investigated in an asymmetric terahertz metasurface integrated with vanadium dioxide (VO_2) using full-wave electromagnetic simulations and coupled-mode theory (CMT). The unit cell consists of two vertical Au bars and one horizontal Au bar, with a VO_2 element positioned in the near-field coupling region. Under normally incident y-polarized THz excitation, the pair of vertical resonators supports a directly excited bright mode, whereas the horizontal resonator supports an indirectly excited dark mode. Gap asymmetry controls the near-field coupling between these modes, thereby enabling the formation and tuning of a pronounced PIT window. At a VO_2 conductivity of σ = 30 S/m and an asymmetry parameter of a_s = 10 μm, two transmission minima at 1.09 and 1.20 THz are separated by a transparency peak at 1.13 THz. As the VO_2 conductivity increases, the PIT response exhibits a distinctly non-monotonic spectral evolution: the low-conductivity transparency window is progressively suppressed in the intermediate-conductivity regime and subsequently re-emerges at a substantially lower frequency in the high-conductivity state. Electromagnetic-field distributions reveal a conductivity-dependent redistribution of the coupled modal response. A conductivity-dependent two-mode CMT model reproduces this spectral evolution and indicates that it originates from the combined variations in bright–dark coupling, modal damping, and resonance detuning, rather than from an increase in ohmic loss alone. These findings provide a physical basis for reconfigurable THz filtering and multistate spectral modulation.

Keywords: non-monotonic plasmon-induced transparency; asymmetric terahertz metasurface; vanadium dioxide; insulator-to-metal transition; coupled-mode theory

1. INTRODUCTION

Electromagnetically induced transparency (EIT) is a quantum interference phenomenon in coherently driven three-level atomic systems, in which destructive interference between excitation pathways produces a narrow transparency window within an otherwise absorptive spectral region (Boller et al. 1991; Harris et al. 1990). The classical analogue of EIT in metamaterials, commonly referred to as PIT, has attracted considerable attention because it enables narrowband transmission filtering, steep phase dispersion, slow-light effects, and high-sensitivity sensing in compact artificial structures (Liu et al. 2009; Papasimakis et al. 2008; Tassin et al. 2009; Zhang et al. 2008). In the terahertz (THz) regime, where natural materials often provide limited electromagnetic functionality, metamaterials offer a versatile platform for engineering resonant transmission, absorption, phase response, and field enhancement through subwavelength structural design (Chen et al. 2006; Chen et al. 2009; Padilla et al. 2007; Tao et al. 2008). Generally, PIT in THz metamaterials is understood as the result of destructive interference between a bright mode and a dark mode. The bright mode is directly excited by the incident THz field, whereas the dark mode is excited indirectly through near-field coupling with the bright mode (Chiam et al. 2009; Singh et al. 2009). Therefore, the PIT response depends sensitively on the modal detuning, radiative and nonradiative damping rates, and coupling strength between the two modes. These quantities are governed by the resonator geometry, including structural asymmetry, inter-resonator spacing, and capacitive gap configuration, as well as by the electromagnetic properties and dissipative losses of the constituent materials. Accordingly, asymmetric planar metasurfaces provide an effective route for controlling the PIT window by tailoring the near-field interaction between bright and dark resonant elements (Hu et al. 2022; Liu et al. 2023; Nourinovin et al. 2023; Tassin et al. 2009).

A major challenge, however, is to extend geometrically fixed PIT structures toward actively tunable operation. Various approaches based on photoconductive semiconductors, graphene, liquid crystals, and microelectromechanical systems have been explored for dynamic THz modulation (Gu et al. 2012; Lee et al. 2012; Pitchappa

et al. 2016; Yin et al. 2018). Among active materials, VO_2 is particularly attractive because it undergoes an insulator-to-metal transition (IMT) near 340 K, accompanied by a conductivity increase of approximately four to five orders of magnitude (a factor of 10^4–10^5) (Berglund and Guggenheim 1969; Morin 1959; Qazilbash et al. 2007; Zylbersztejn and Mott 1975). The integration of VO_2 with THz metamaterials has enabled resonance switching, tunable absorption, amplitude modulation, and active control of EIT-like or PIT responses (Driscoll et al. 2009; Jiang et al. 2022; Li et al. 2019; Lu et al. 2021; Wang et al. 2017). Several previous VO_2-based EIT/PIT studies have primarily demonstrated switching or monotonic modulation of the transparency response as the VO_2 conductivity is varied (Chen et al. 2020; Ma et al. 2023). Comparatively less attention has been devoted to how the PIT coupling condition evolves continuously through the intermediate-conductivity regime, where conductivity-induced variations in resonance detuning, modal damping, and near-field coupling may occur simultaneously.

In this work, we investigate an asymmetric VO_2-integrated THz metasurface that exhibits a non-monotonic conductivity-dependent PIT response. The gap asymmetry controls the near-field interaction between the directly excited bright mode supported by the vertical resonators and the indirectly excited dark mode supported by the horizontal resonator, enabling the formation and systematic tuning of the PIT window. At a fixed asymmetry, increasing the VO_2 conductivity drives the system from a pronounced low-conductivity PIT state to an intermediate regime in which the transparency window is suppressed, followed by the re-emergence of a substantially redshifted PIT window at high conductivity. The associated field distributions reveal the redistribution of electromagnetic-field localization among the coupled elements and are consistent with an interference-mediated transparency mechanism. A conductivity-dependent two-mode CMT model is further employed to describe the spectral evolution in terms of the combined changes in bright–dark coupling, modal damping, and resonance detuning. These results demonstrate that the active PIT response cannot be explained by conductivity-induced dissipation alone, but instead arises from the coupled evolution of the resonant parameters. The proposed approach provides a route toward reconfigurable THz filtering and multistate spectral modulation.

2. STRUCTURE DESIGN AND NUMERICAL MODEL

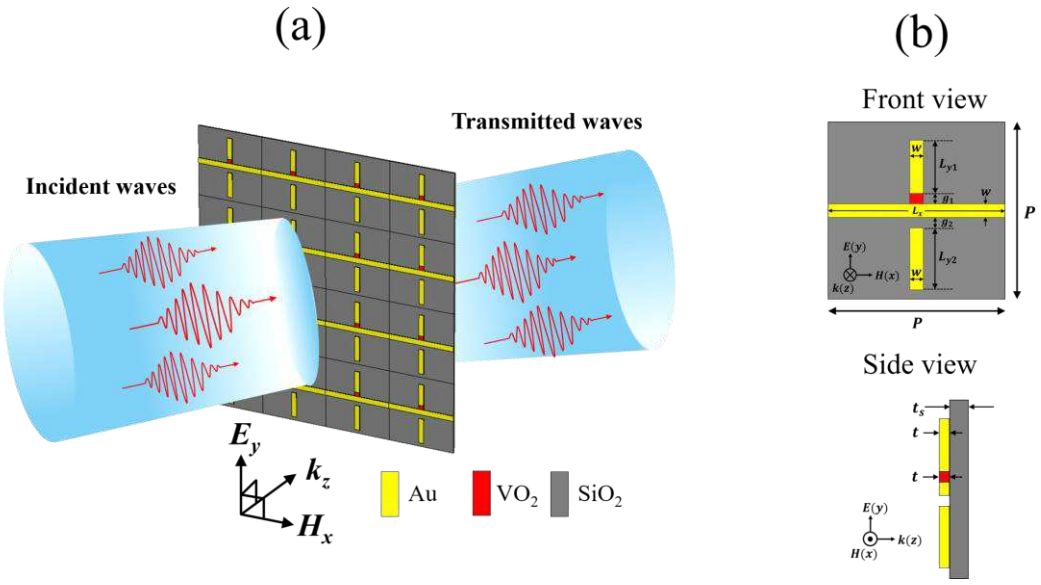


Fig. 1. (a) Schematic of THz-wave transmission through the proposed VO_2-integrated metasurface. (b) Front and side views of the unit cell consisting of two vertical Au resonators and one horizontal Au resonator on a quartz substrate, with a VO_2 patch filling in the upper coupling gap g_1.

Figure 1(a) illustrates the proposed VO_2-integrated THz metasurface under normally incident y-polarized excitation, while Fig. 1(b) shows the front and side views of the unit cell. The unit cell consists of two vertical Au resonators and one horizontal Au resonator patterned on a quartz (SiO_2) substrate. The pair of vertical resonators supports the directly excited bright mode, whereas the horizontal bar supports a weakly radiative dark mode that is indirectly excited through near-field coupling, as demonstrated in Sec. 3. The quartz substrate has a relative permittivity of 3.75, a loss tangent of 0.0004 (Chen et al. 2022; Sabah et al. 2014), and a thickness of $4\ \mu m$. Au was modeled as a lossy metal with an electrical conductivity of $\sigma_{Au} = 4.09 \times 10^7$ S/m. A VO_2 patch fills the upper coupling gap g_1 between the upper vertical resonator and the horizontal resonator, whereas the lower coupling region remains an air gap g_2. The upper gap is fixed at $g_1 = 12\ \mu$m, whereas g_2 is varied from 12 to 0 μm; $g_2 = 0$ corresponds to direct contact between the lower vertical and horizontal Au resonators. The gap asymmetry parameter is defined as $a_s = g_1 - g_2$, where $a_s = 0$ denotes the equal-gap configuration and $0 \le a_s \le 12\ \mu$m describes increasing gap asymmetry. The VO_2 patch fills the upper gap and has in-plane dimensions $w \times g_1$. The geometric

parameters are $P = 200\ \mu\text{m}$, $L_x = 200\ \mu\text{m}$, $L_{y1} = 60\ \mu\text{m}, L_{y2} = 70\ \mu\text{m}$, and $w = 15\ \mu\text{m}$. Both Au resonators and the VO_2 patch have a thickness of $t = t_{VO_2} = 2\ \mu\text{m}$. The complex relative permittivity VO_2 was modeled using a conductivity-dependent Drude model (Li et al. 2019; Wang et al. 2017)

$$\varepsilon_{\text{VO}_2}(\omega, \sigma) = \varepsilon_\infty - \frac{\omega_p^2(\sigma)}{\omega^2 + i\gamma\omega}. \quad (1)$$

Here, $\varepsilon_\infty = 12$ is the high-frequency relative permittivity and $\gamma = 5.75 \times 10^{13}\ \text{rad/s}$ is the carrier damping rate. The conductivity-dependent plasma frequency is given by

$$\omega_p^2(\sigma) = \omega_p^2(\sigma_0)\frac{\sigma}{\sigma_0}, \quad (2)$$

where σ denotes the effective dc conductivity parameter used to describe the conductivity-dependent electromagnetic response of VO_2. The metallic reference parameters are $\omega_p(\sigma_0) = 1.40 \times 10^{15}\ \text{rad/s}$ and $\sigma_0 = 3.0 \times 10^5\ \text{S/m}$ (Li et al. 2019; Wang et al. 2017). In the simulations, σ was varied from 30 to $3.0 \times 10^5\ \text{S/m}$ effective conductivity states spanning the low- to high-conductivity regimes of VO_2. Full-wave electromagnetic simulations were performed using the frequency-domain solver based on the finite element method (FEM) in CST Studio Suite. Periodic boundary conditions were applied along the x- and y-directions to represent an infinitely periodic metasurface. A normally incident THz wave propagating along the z-direction was used to excite the structure, with the electric field polarized along the y-direction, as shown in Fig. 1(a). Tetrahedral meshing was employed to discretize the computational domain and represent the metallic resonators, VO_2 patch, and dielectric substrate.

3. RESULTS AND DISCUSSION

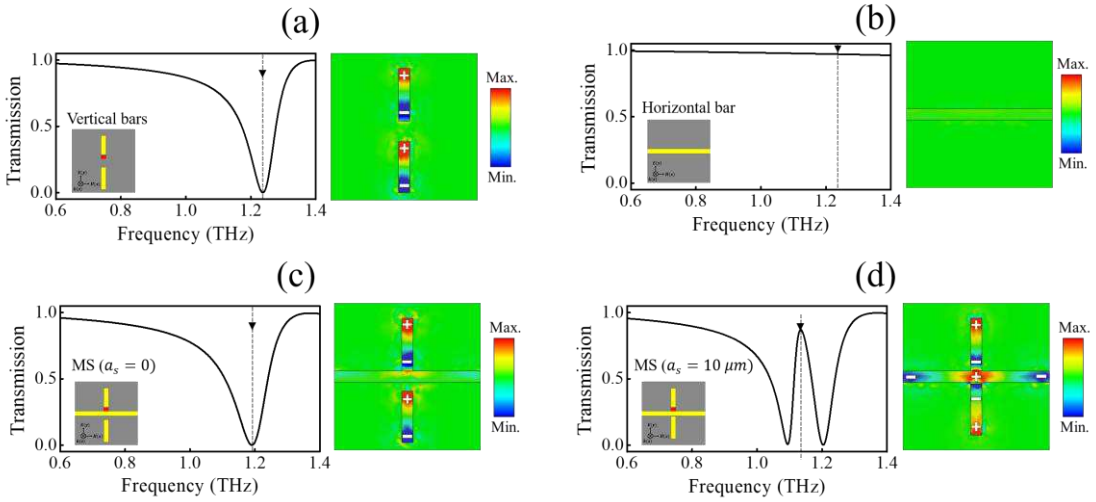


Fig. 2 Transmission spectra and corresponding electric-field distributions under normally incident y-polarized THz excitation for (a) isolated vertical Au resonators, (b) an isolated horizontal Au resonator, (c) the equal-gap coupled structure ($a_s = 0$), and (d) the gap-asymmetric VO_2-integrated coupled structure ($a_s = 10\ \mu$m). For the coupled structures, the VO_2 conductivity is fixed at $\sigma = 30$ S/m. The electric-field distributions are evaluated at the frequencies indicated by the arrows in the corresponding transmission spectra.

Figure 2 illustrates the modal response of the VO_2-integrated metasurface at a fixed VO_2 conductivity of $\sigma = 30$ S/m. In Fig. 2(a), the isolated vertical Au resonators are directly excited by the normally incident y-polarized THz wave and exhibit a bright electric-dipole resonance at 1.24 THz. The corresponding electric-field distribution shows strong field localization near the inner ends of the vertical resonators, consistent with a directly excited electric-dipole-like resonance. Because only the vertical resonators are present, bright–dark mode coupling is absent in this configuration. Figure 2(b) shows the electric-field response of the isolated horizontal Au resonator at 1.24 THz. Because its longitudinal axis is perpendicular to the incident electric field, direct electric-dipole excitation is strongly suppressed. The weak direct response indicates that the horizontal resonator is inefficiently excited by the incident y-polarized field and can therefore participate as a dark resonator when coupled to the vertical bright resonators.

When the vertical and horizontal resonators are combined in the equal-gap configuration ($a_s = 0$), the dominant resonance redshifts from 1.24 to 1.19 THz, consistent with the modified electromagnetic environment and mutual loading introduced by the coupled geometry. However, no distinct PIT window is resolved, indicating that the bright–dark interaction in the equal-gap configuration is insufficient to generate a resolvable transparency feature. In contrast, increasing the gap asymmetry modifies the near-field interaction between the vertical and horizontal resonators, enabling more effective excitation of the dark response and producing a distinct PIT window [Fig. 2(d)]. Because the VO_2 conductivity is fixed at $\sigma = 30$ S/m, the spectral evolution from Fig. 2(c) to Fig. 2(d) directly demonstrates the role of gap asymmetry in modifying the bright–dark near-field coupling and establishing the PIT response.

Based on the modal characteristics identified in Fig. 2, the physical origin of the PIT window can be interpreted using a three-level EIT-like modal analogy (Kim et al. 2023; Tassin et al. 2012), in which $|0\rangle$, $|B\rangle$, and $|D\rangle$denote the ground-state, bright-state, and dark-state analogues, respectively. The pair of directly excited vertical resonators supports the bright mode, whereas the horizontal resonator supports the dark mode, which is excited indirectly through near-field coupling. In the corresponding classical modal description, $B(\omega)$and $D(\omega)$denote the complex amplitudes of the bright and dark modes, with resonance frequencies $\omega_B$and $\omega_D$and damping rates $\gamma_B$and γ_D, respectively. Gap asymmetry controls the near-field coupling between the two modes, allowing the dark-mode-mediated response to interfere with the directly driven radiative response of the bright mode. At the transparency frequency, the resulting destructive interference suppresses the net radiative response of the bright mode, thereby producing the PIT window. To quantitatively describe the coupled modal response and its dependence on gap asymmetry and VO_2 conductivity, a two-mode CMT model is introduced (Fu et al. 2017; Kim et al. 2025; Tassin et al. 2012):

$$\begin{bmatrix} \omega - \omega_B(\sigma) - i\gamma_B(\sigma) & \kappa(a_s,\sigma) \\ \kappa(a_s,\sigma) & \omega - \omega_D(\sigma) - i\gamma_D(\sigma) \end{bmatrix} \begin{bmatrix} B \\ D \end{bmatrix} = \begin{bmatrix} gE \\ 0 \end{bmatrix}, \tag{3}$$

Here, B and D are the complex amplitudes of the bright and dark modes, respectively; ω_B and ω_D are their resonance frequencies; γ_B and γ_D are the corresponding effective damping rates; κ is the effective bright–dark coupling coefficient; and g describes the coupling between the incident-field amplitude E_0 and the bright mode.

An implicit $e^{i\omega t}$ time dependence is assumed. All modal parameters may depend on both the gap-asymmetry parameter a_s and the VO_2 conductivity σ; their explicit arguments are omitted hereafter for clarity. Solving Eq. (3) for the bright-mode response and assuming a unit non-resonant background transmission, the normalized power transmission is phenomenologically expressed as

$$T(\omega, a_s, \sigma) = 1 - \left| \frac{g[\omega - \omega_D - i\gamma_D]}{(\omega - \omega_B - i\gamma_B)(\omega - \omega_D - i\gamma_D) - \kappa^2} \right|^2 \tag{4}$$

Here, $T(\omega, a_s, \sigma)$ denotes the normalized power transmission, where the second term represents the resonant attenuation contribution relative to the unit background transmission. Within this model, the PIT response is governed by the interplay among the bright–dark coupling κ, the modal damping rates γ_B and γ_D, and the resonance detuning $|\omega_B - \omega_D|$. Gap asymmetry modifies the modal interaction, including the effective bright–dark coupling and damping, whereas variations in VO_2 conductivity can simultaneously alter the coupling strength, modal damping, and resonance frequencies. Accordingly, the conductivity-dependent PIT evolution is governed by the combined variations in coupling, damping, and resonance detuning rather than by conductivity-induced dissipation alone. The applicability of the coupled-mode model is evaluated in the low-conductivity VO_2 state by comparing the CMT-derived and full-wave simulated transmission spectra.

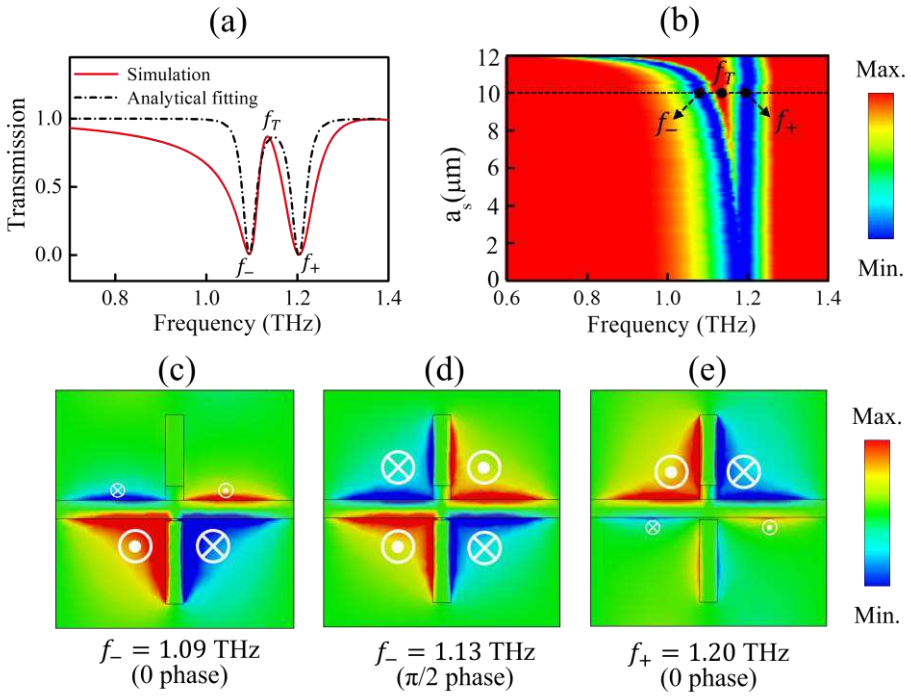


Fig. 3 PIT formation in the asymmetric VO_2-integrated metasurface in the low-conductivity VO_2 state (σ = 30 S/m). (a) Simulated (red solid) and analytically fitted (black dashed-dotted line) transmission spectra at $a_s = 10\ \mu$m, with valleys at $f_- = 1.09$ THz and $f_+ = 1.20$ THz and a PIT peak at $f_T = 1.13$ THz. (b) Simulated transmission as a function of frequency and gap-asymmetry parameter a_s under y-polarized normal incidence. (c)–(e) Out-of-plane magnetic-field (H_z) distributions at f_-, f_T, and f_+, respectively, where $\otimes$ and $\odot$ denote the $-z$ and $+z$ directions of H_z.

Figure 3 presents the response of the gap-asymmetric metasurface in the low-conductivity VO_2 state ($\sigma = 30$ S/m). At $a_s = 10\ \mu$m, the transmission spectrum in Fig. 3(a) exhibits a pronounced PIT window, with two transmission minima at $f_- = 1.09$ THz and $f_+ = 1.20$ THz separated by a transparency peak at $f_T = 1.13$ THz. The analytically fitted spectrum qualitatively reproduces the main spectral features of the full-wave simulation, including the two transmission minima and the intervening transparency peak, although some discrepancies remain in the spectral line shape and resonance linewidths owing to the simplified two-mode description. The dependence of the PIT response on gap asymmetry is shown in Fig. 3(b), which maps the simulated transmission as a function of frequency and $a_s$under normally incident y-polarized

excitation. At $a_s = 0$, the spectrum exhibits a single broad low-transmission band without a resolvable transparency window. As a_s increases, a transparency peak progressively develops, while the separation between the two transmission minima increases. This spectral evolution demonstrates that gap asymmetry controls the formation and spectral separation of the PIT response by modifying the near-field interaction between the bright and dark resonant modes. The dashed line at $a_s = 10\ \mu$mcorresponds to the operating condition in Fig. 3(a), where f_-, f_T, and $f_+$are indicated. The out-of-plane magnetic-field (H_z) distributions in Figs. 3(c)–3(e) further resolve the modal character at the three characteristic frequencies, where $\otimes$ and $\odot$ denote the $-z$ and $+z$ directions of H_z, respectively. At the lower- and higher-frequency transmission minima, $f_- = 1.09$ THz and $f_+ = 1.20$ THz, the magnetic response extends over both the vertical and horizontal resonators, reflecting the coupled character of these resonant states. In contrast, at the transparency peak $f_T = 1.13$THz, the magnetic response is strongly localized around the horizontal dark resonator, indicating enhanced excitation of the dark mode. This redistribution of the resonant field is consistent with the bright–dark interference mechanism underlying the PIT window.

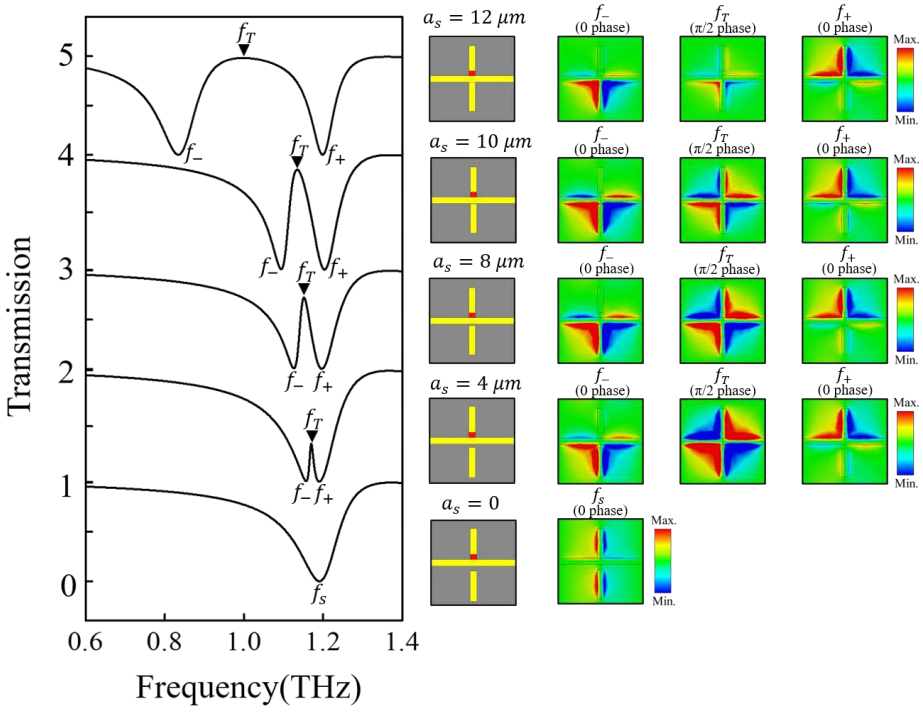


Fig. 4 Transmission spectra and magnetic-field (H_z) distributions of the VO_2-integrated metasurface as a function of the gap-asymmetry parameter at a fixed

VO_2 conductivity of σ = 30 S/m under normally incident y-polarized waves. Successive transmission spectra are vertically offset by one unit for clarity. The evolution from a single resonance in the equal-gap configuration ($a_s = 0$) to a PIT window with increasing gap asymmetry is accompanied by redistribution of the magnetic field at the characteristic frequencies f_-, f_T, and f_+.

Figure 4 shows the transmission spectra and magnetic-field (H_z) distributions of the VO_2-integrated metasurface as a function of the asymmetry parameter at a fixed VO_2 conductivity of σ = 30 S/m. For the equal-gap configuration ($a_s = 0$), the spectrum exhibits a single transmission minimum at f_s, without a resolvable PIT window. The corresponding H_z distribution is consistent with a response dominated by the directly excited bright mode. As a_s increases from zero, the unequal gap widths modify the near-field interaction between the bright vertical and dark horizontal resonant responses. As a result, the single resonant feature evolves into two transmission valleys, f_- and f_+, with a transparency peak f_T developing between them. This progressive spectral evolution reflects the asymmetry-induced modification of the coupled bright–dark response. The magnetic field distributions further support this interpretation. At f_- and f_+, the magnetic-field is strongly localized around the coupled resonators, consistent with coupled bright–dark resonant responses. In contrast, at the transparency frequency f_T, the H_z distribution differs markedly from those at the two transmission valleys and exhibits enhanced localization around the horizontal dark resonator. This modal-field redistribution is consistent with the bright–dark interference mechanism underlying the PIT window. Within the investigated range, increasing a_s from 4 to 12 μm progressively enhances the PIT peak transmission and increases the separation between the two transmission valleys, demonstrating effective gap-asymmetry control of the transparency response. However, this transmission enhancement is accompanied by a reduction in the Q-factor, indicating a trade-off between peak transmission and spectral selectivity.

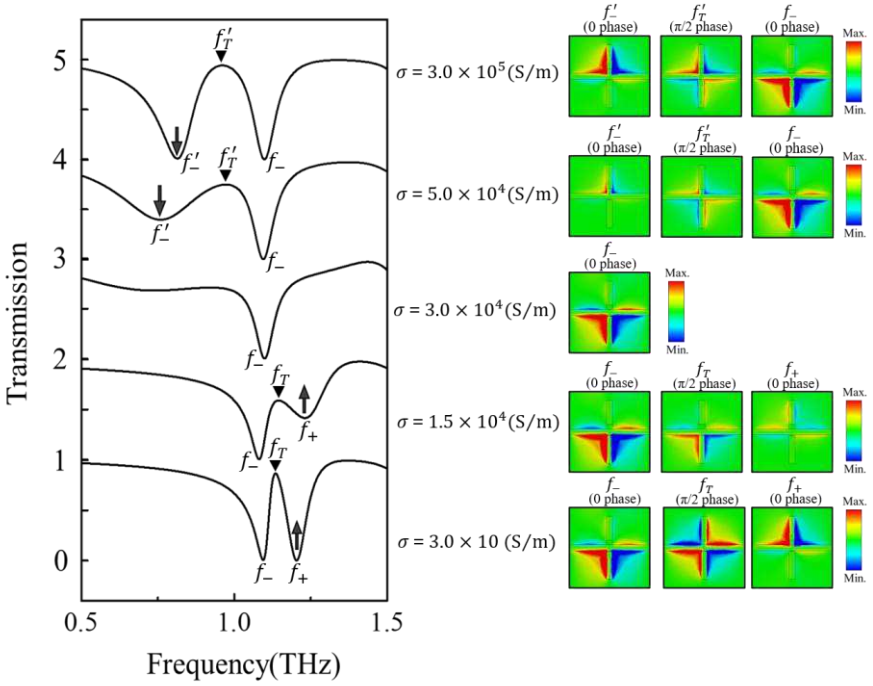


Fig. 5 Transmission spectra and out-of-plane magnetic-field (H_z) distributions of the VO_2-integrated metasurface as a function of VO_2 conductivity at a fixed gap-asymmetry parameter of $a_s = 10\ \mu$munder normally incident y-polarized THz excitation. Successive transmission spectra are vertically offset by one unit for clarity. The low-conductivity PIT window, characterized by f_-, f_T, and f_+, is progressively suppressed in the intermediate-conductivity regime. At high conductivity, a lower-frequency PIT window re-emerges, consisting of a newly developed lower-frequency minimum f_-', a transparency peak f_T', and the persistent f_- branch, which forms the higher-frequency minimum of the re-emergent PIT response.

Figure 5 shows the conductivity-dependent evolution of the PIT response at a fixed gap-asymmetry parameter of $a_s = 10\ \mu$m. Here, f_-, f_T, and f_+ denote the lower-frequency transmission valley, transparency peak, and higher-frequency transmission valley of the PIT window formed in the low-conductivity VO_2 state, respectively. At $\sigma = 30$ S/m, a pronounced PIT window is observed between the two transmission valleys f_- and f_+. The corresponding H_z distributions exhibit localized resonant responses at the two transmission valleys, whereas the field pattern at f_T is distinctly redistributed, consistent with the bright–dark interference mechanism underlying the transparency. As the VO_2 conductivity increases to 1.5×10^4 and 3.0×10^4 S/m, the

original PIT window is progressively suppressed. In particular, the higher-frequency minimum f_+ becomes increasingly weak, whereas the f_- branch remains dominant, causing the spectrum to evolve toward a single pronounced transmission minimum. This suppression is consistent with conductivity-induced modification of the local electromagnetic loading, which alters the effective bright–dark coupling, modal damping, and resonance detuning. At higher conductivities of 5.0×10^4 and 3.0×10^5 S/m, a lower-frequency PIT window re-emerges. Importantly, this response does not correspond to a simple redshift of the original PIT window. Instead, the original lower-frequency branch f_- persists and forms the higher-frequency minimum of the re-emergent PIT window, while a new lower-frequency branch f_-' develops and a new transparency peak f_T' appears between them. The corresponding H_z distributions at f_-' and f_- show localized resonant responses, whereas the field redistribution at f_T' is consistent with bright–dark interference associated with the re-emergent transparency window. The spectral evolution in Fig. 5 therefore demonstrates a distinctly non-monotonic conductivity-dependent PIT response: the low-conductivity PIT window is suppressed in the intermediate-conductivity regime and subsequently re-emerges at a substantially lower frequency in the high-conductivity state through a reconfiguration of the coupled resonant branches. At fixed gap-asymmetry, this non-monotonic behavior arises from the coupled conductivity-dependent evolution of bright–dark coupling, modal damping, and resonance detuning, rather than from conductivity-induced dissipation alone. The associated phase and group-delay responses, together with the fitted CMT parameters, are examined below to further clarify this non-monotonic PIT evolution.

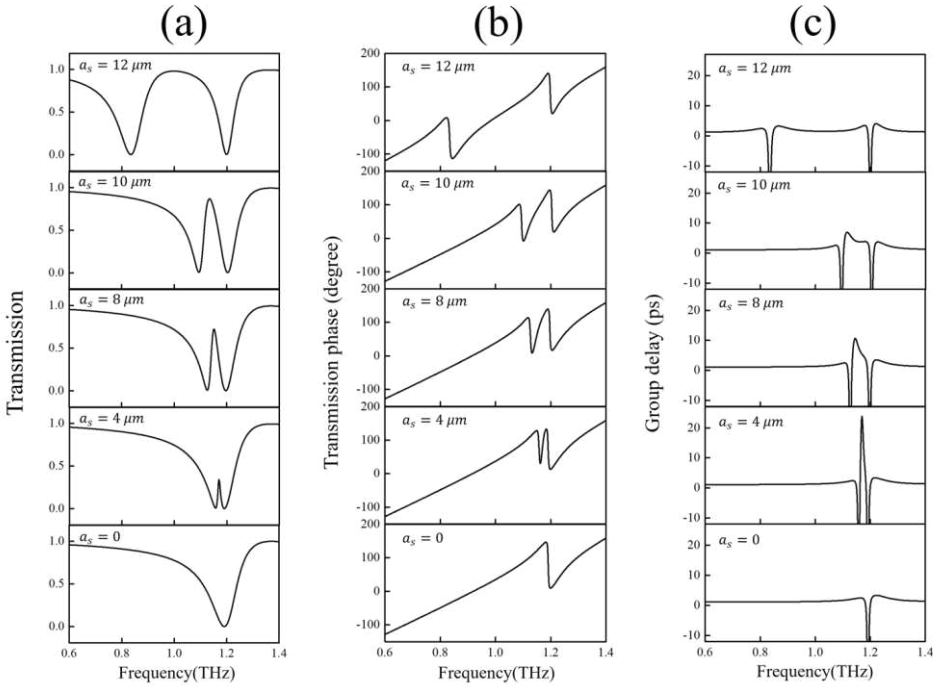


Fig. 6 (a) Transmission spectra, (b) transmission phase, and (c) group delay of the VO_2-integrated metasurface for different gap-asymmetry parameters (a_s = 0, 4, 8, 10, and 12 μm) at a fixed VO_2 conductivity of σ = 30 S/m under normally incident y-polarized THz waves.

Figure 6 shows the transmission spectrum, transmission phase, and group delay of the VO_2-integrated metasurface as a function of the asymmetry parameter at a fixed VO_2 conductivity of $\sigma = 30\,\mathrm{S/m}$. For the equal gap configuration ($a_s = 0$), a single transmission valley is observed at 1.19 THz, accompanied by a comparatively weak dispersive phase response. As a_s increases, the transparency peak becomes progressively more pronounced and the two transmission valleys become more clearly separated, consistent with the PIT evolution discussed above. This spectral evolution is accompanied by pronounced phase dispersion near the characteristic frequencies. Using the $e^{i\omega t}$ time convention adopted above, the group delay of the transmitted wave is evaluated from the transmission phase according to

$$\tau_g = -\frac{d\phi(\omega)}{d\omega} \tag{5}$$

where $\phi(\omega)$ is the transmission phase and $\omega = 2\pi f$ is the angular frequency. The transmission phase was unwrapped and expressed in radians prior to numerical

differentiation. The pronounced phase dispersion associated with the PIT response gives rise to corresponding group-delay features, consistent with the dispersive behavior characteristic of EIT/PIT-like resonant systems (Bilal et al. 2020; He et al. 2017; Li et al. 2023). Increasing gap asymmetry enhances the PIT window but does not monotonically increase the group delay, consistent with the accompanying resonance broadening and reduction in Q factor. Thus, gap asymmetry governs both the spectral and dispersive characteristics of the PIT response. Thus, at fixed low VO_2 conductivity, gap asymmetry controls not only the spectral formation of the PIT window but also its associated phase dispersion and group-delay characteristics.

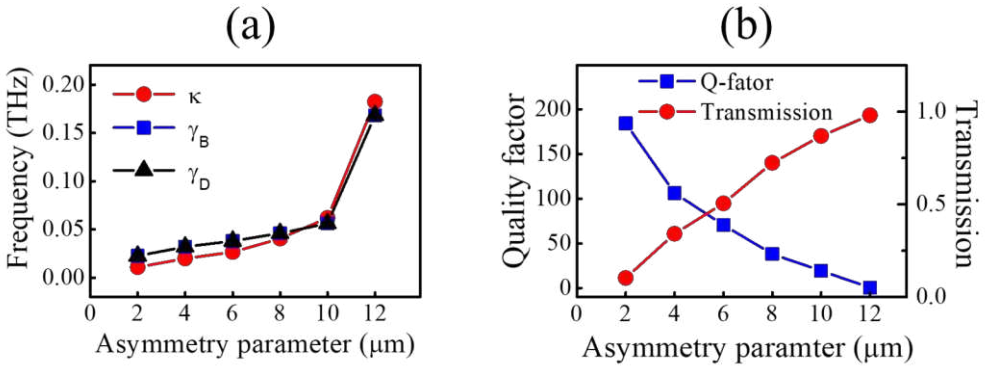


Fig. 7 (a) Fitted effective coupling coefficient (κ) and damping rates (γ_B and γ_D) as functions of the asymmetry parameter a_s. (b) Q-factor and maximum transmission of the PIT peak as functions of $a_s$for the VO_2-integrated metasurface at a fixed conductivity of $\sigma = 30$ S/m under normally incident y-polarized THz waves.

Figure 7 quantitatively examines the influence of gap asymmetry on the effective coupled-mode parameters and PIT characteristics at $\sigma = 30$ S/m. The effective coupling coefficient κ and damping rates γ_B and γ_D were obtained as parameters by applying the two-mode CMT model to the simulated transmission spectra at each a_s. As shown in Fig. 7(a), the fitted κ increases with gap asymmetry, indicating enhanced effective bright–dark modal interaction. The fitted damping rates exhibit a similar increasing trend. These parameters vary relatively gradually up to $a_s = 10\ \mu$m, whereas a pronounced increase occurs at $a_s = 12\ \mu$m. At this limiting condition, $g_2 = 0$ and the lower vertical and horizontal Au elements become directly connected;

therefore, the abrupt parameter change reflects not only increased gap asymmetry but also the transition from gap-mediated coupling to direct electrical connectivity. The Q-factor was evaluated as $\mathrm{Q} = f_T/\mathrm{FWHM}$, where FWHM denotes the full width at half maximum of the transparency peak (Bilal et al. 2020). As shown in Fig. 7(b), the maximum PIT transmission increases monotonically with a_s, approaching unity at the largest asymmetry, whereas the Q-factor decreases substantially. This opposite evolution reveals a trade-off between peak transmission and spectral selectivity. A similar dependence of the transparency response on gap asymmetry has been reported in THz EIT-like metamaterials (He et al. 2020). Increasing gap asymmetry enhances the PIT transmission but also increases the fitted damping rates, leading to resonance broadening and a reduced Q factor. Thus, the observed trade-off between peak transmission and spectral selectivity results from the competing effects of enhanced bright–dark coupling and increased modal damping.

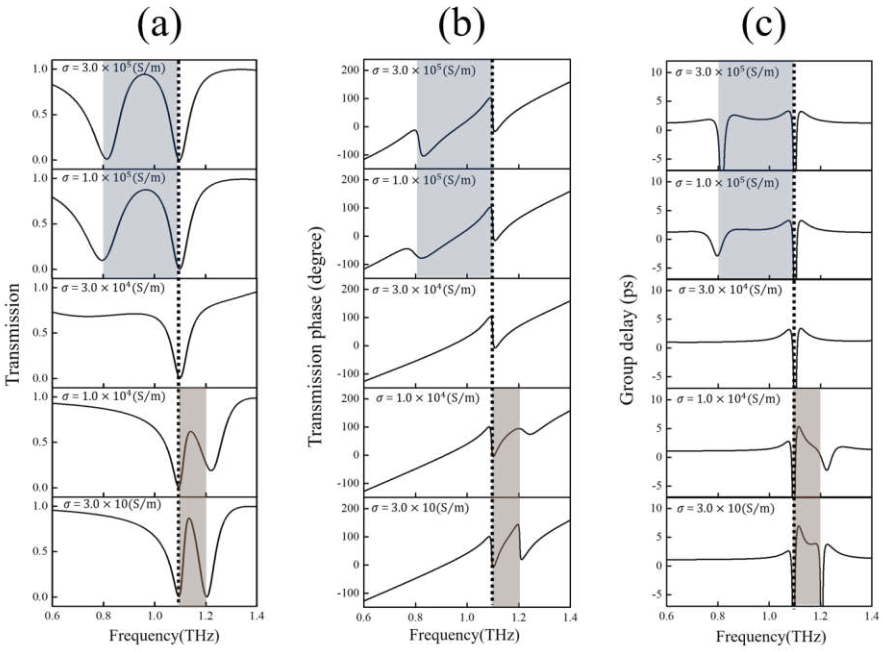


Fig. 8 (a) Transmission spectra, (b) transmission phase, and (c) corresponding group delay of the VO_2-integrated metasurface at representative VO_2 conductivities of $\sigma = 30$, 1.0×10^4, 3.0×10^4, 1.0×10^5, and 3.0×10^5 S/m, for a fixed gap-asymmetry parameter of $a_s = 10\ \mu$m under normally incident y-polarized THz excitation.

Figure 8 shows the conductivity-dependent evolution of the transmission, transmission phase, and group-delay responses at a fixed gap-asymmetry parameter of $a_s = 10\ \mu$m. In the low-conductivity state ($\sigma = 30$ S/m), a pronounced PIT window appears between two transmission valleys. The corresponding transmission phase exhibits strong dispersion across the transparency region, accompanied by a positive group-delay response in the high transmission region. These features are consistent with the interference-mediated PIT response identified above. As conductivity increases to $\sigma = 1.0 \times 10^4$S/m, the transparency peak is reduced, and the associated phase dispersion becomes weaker. At $\sigma = 3.0 \times 10^4$S/m, the PIT window is largely suppressed, and the spectrum is dominated by a single pronounced resonance near the persistent branch around 1.1 THz. Correspondingly, the characteristic phase dispersion structure and positive group delay feature associated with the PIT window are substantially weakened. This evolution is consistent with suppression of the interference mediated PIT response in the intermediate-conductivity regime. At higher conductivities of $\sigma = 1.0 \times 10^5$ and 3.0×10^5 S/m, an additional low-frequency resonance develops near 0.8 THz while the persistent branch near 1.1 THz remains, producing a new high transmission region between the two resonances. The corresponding phase spectra recover pronounced dispersion across this newly formed transparency region, together with a positive group delay response. These correlated spectral, phase, and group delay features are consistent with the re-emergence of an interference-mediated PIT response at a substantially lower frequency. Importantly, this behavior represents a reconfiguration of the coupled resonant branches rather than a simple redshift of the original PIT window.

4. CONCLUSION

In summary, we investigated non-monotonic plasmon-induced transparency in an asymmetric VO_2-integrated terahertz metasurface through full-wave simulations and coupled-mode analysis. The pair of vertical Au resonators supports a directly excited bright mode, whereas the horizontal resonator supports an indirectly excited dark mode; gap asymmetry controls the near-field coupling between these modes and enables the formation of a PIT window. At $\sigma = 30\ \mathrm{S/m}$ and $a_s = 10\ \mu\mathrm{m}$, a transparency peak at 1.13 THz appears between two transmission minima at 1.09 and 1.20 THz. Increasing the gap asymmetry enhances the PIT transmission while reducing the Q-factor, revealing a trade-off between peak transmission and spectral selectivity. More importantly, the PIT response evolves non-monotonically with VO_2 conductivity: the low-conductivity PIT window is progressively suppressed in the intermediate-conductivity regime and subsequently re-emerges at a substantially lower frequency in the high-conductivity state. The corresponding field distributions, phase dispersion, and group-delay characteristics are consistent with bright–dark interference underlying the re-emergent PIT window. Within the conductivity-dependent two-mode CMT model, this behavior arises from the combined evolution of bright–dark coupling, modal damping, and resonance detuning rather than from conductivity-induced dissipation alone. These findings provide a physical basis for reconfigurable THz filtering and multistate spectral modulation.

Statements and Declarations

Funding

This work was supported by the Hankuk University of Foreign Studies Research Fund of 2026 and by the National Research Foundation of Korea (NRF) grant funded by the Korean government (MSIT) under the Mid-Career Research Program (Creative Research) (No. RS-2025-16070436).

Competing Interests

The authors have no relevant financial or non-financial interests to disclose.

Author Contributions

T.-H. Kim: Conceptualization, formal analysis, methodology, software, validation, visualization, and writing – original draft. J.H. Seo: Formal analysis, validation, and writing – review and editing. Y.J. In: Software, validation, and writing – review and editing. D.G. Lee: Software, validation, and writing – review and editing. B.W. Lee: Project administration, supervision, and writing – review and editing. All authors discussed the results, reviewed the manuscript, and approved the final version.

Data Availability

The data generated and/or analyzed during the current study are available from the corresponding author upon reasonable request.

References

Berglund, C.N., Guggenheim, H.J.: Electronic properties of VO_2 near the semiconductor-metal transition. Phys. Rev. **185**, 1022–1033 (1969). https://doi.org/10.1103/PhysRev.185.1022

Bilal, R.M.H., Baqir, M.A., Choudhury, P.K., Ali, M.M., Rahim, A.A.: Tunable and multiple plasmon-induced transparency in a metasurface comprised of silver S-shaped resonator and rectangular strip. IEEE Photonics J. **12**, 4500613 (2020). https://doi.org/10.1109/JPHOT.2020.2988698

Boller, K.-J., Imamoğlu, A., Harris, S.E.: Observation of electromagnetically induced transparency. Phys. Rev. Lett. **66**, 2593–2596 (1991).

https://doi.org/10.1103/PhysRevLett.66.2593

Chen, H.-T., Padilla, W.J., Zide, J.M.O., Gossard, A.C., Taylor, A.J., Averitt, R.D.: Active terahertz metamaterial devices. Nature **444**, 597–600 (2006).

https://doi.org/10.1038/nature05343

Chen, H.-T., Padilla, W.J., Cich, M.J., Azad, A.K., Averitt, R.D., Taylor, A.J.: A metamaterial solid-state terahertz phase modulator. Nat. Photonics **3**, 148–151 (2009). https://doi.org/10.1038/nphoton.2009.3

Chen, M., Xiao, Z., Lu, X., Lv, F., Cui, Z., Xu, Q.: Dynamically tunable multi-resonance and polarization-insensitive electromagnetically induced transparency-like based on vanadium dioxide film. Opt. Mater. **102**, 109811 (2020). https://doi.org/10.1016/j.optmat.2020.109811

Chen, Z.-M., et al.: High-efficiency miniaturized spoof plasmonic waveguide filter from direct current to millimeter-wave frequency. Adv. Photonics Res. **3**, 2100205 (2022). https://doi.org/10.1002/adpr.202100205

Chiam, S.-Y., et al.: Analogue of electromagnetically induced transparency in a terahertz metamaterial. Phys. Rev. B **80**, 153103 (2009).

https://doi.org/10.1103/PhysRevB.80.153103

Driscoll, T., et al.: Memory metamaterials. Science **325**, 1518–1521 (2009). https://doi.org/10.1126/science.1176580

Fu, Q., Zhang, F., Fan, Y., Dong, J., Cai, W., Zhu, W., Chen, S., Yang, R.: Weak coupling between bright and dark resonators with electrical tunability and analysis based on temporal coupled-mode theory. Appl. Phys. Lett. **110**, 221905 (2017). https://doi.org/10.1063/1.4984596

Gu, J., et al.: Active control of electromagnetically induced transparency analogue in terahertz metamaterials. Nat. Commun. **3**, 1151 (2012).

https://doi.org/10.1038/ncomms2153

Harris, S.E., Field, J.E., Imamoğlu, A.: Nonlinear optical processes using electromagnetically induced transparency. Phys. Rev. Lett. **64**, 1107–1110 (1990).

https://doi.org/10.1103/PhysRevLett.64.1107

He, X., Huang, Y., Yang, X., Zhu, L., Wu, F., Jiang, J.: Tunable electromagnetically induced transparency based on terahertz graphene metamaterial. RSC Adv. **7**, 40321–40326 (2017). https://doi.org/10.1039/C7RA06770D

He, Y., Wang, B.-X., Lou, P., Xu, N., Wang, X., Wang, Y., Cao, J.: Convert from Fano resonance to electromagnetically induced transparency effect using anti-symmetric H-typed metamaterial resonator. Opt. Quantum Electron. **52**, 391 (2020). https://doi.org/10.1007/s11082-020-02513-3

Hu, Y., Xiong, Y.: High-Q and tunable analog of electromagnetically induced transparency in terahertz all-dielectric metamaterial. Appl. Opt. **61**, 1500–1506 (2022). https://doi.org/10.1364/AO.447262

Jiang, H., et al.: Vanadium dioxide-based terahertz metamaterial devices switchable between transmission and absorption. Micromachines **13**, 715 (2022).

https://doi.org/10.3390/mi13050715

Kim, T.-H., Yoo, Y.J., Park, S.Y., Lee, B.W.: Analog of electromagnetically induced transparency based on asymmetric nickel-ferrite metamaterials in THz regime. AIP Adv. **13**, 075206 (2023). https://doi.org/10.1063/5.0146706

Kim, T.-H., Kim, S.W., Lee, B.W.: Tunable plasmon-induced transparency based on graphene metasurface structure for mid-infrared sensing applications. Curr. Appl. Phys. **73**, 30–40 (2025). https://doi.org/10.1016/j.cap.2025.02.009

Lee, S.H., et al.: Switching terahertz waves with gate-controlled active graphene metamaterials. Nat. Mater. **11**, 936–941 (2012). https://doi.org/10.1038/nmat3433

Li, H., Xu, Z., Wang, H., Chen, J.: An actively tunable multifrequency electromagnetically induced transparency in a terahertz metamaterial. Opt. Quantum Electron. **55**, 198 (2023). https://doi.org/10.1007/s11082-022-04472-3

Li, X., et al.: Switchable multifunctional terahertz metasurfaces employing vanadium dioxide. Sci. Rep. **9**, 5454 (2019). https://doi.org/10.1038/s41598-019-41915-6

Liu, C., et al.: Tailoring electromagnetic responses in terahertz metasurface by breaking the structural symmetry in T-shaped resonators. Adv. Photonics Res. **4**, 2200356 (2023). https://doi.org/10.1002/adpr.202200356

Liu, N., et al.: Plasmonic analogue of electromagnetically induced transparency at the Drude damping limit. Nat. Mater. **8**, 758–762 (2009).

https://doi.org/10.1038/nmat2495

Lu, X., et al.: Two-channel VO_2 memory meta-device for terahertz waves. Nanomaterials **11**, 3409 (2021). https://doi.org/10.3390/nano11123409

Ma, Y., Huang, L., Chen, L.: Active control of broadband plasmon induced transparency window and amplitude modulation based on embedded-vanadium-dioxide metamaterials. Opt. Commun. **545**, 129706 (2023).

https://doi.org/10.1016/j.optcom.2023.129706

Morin, F.J.: Oxides which show a metal-to-insulator transition at the Neel temperature. Phys. Rev. Lett. **3**, 34–36 (1959). https://doi.org/10.1103/PhysRevLett.3.34

Nie, S., Wang, J., Li, X., Cai, K., Sun, P., Zhou, Y., Su, L., Gao, Y.: Application of graphene-based metasurface plasma-induced transparency in terahertz band optical switches. Opt. Commun. **569**, 130859 (2024).

https://doi.org/10.1016/j.optcom.2024.130859

Nourinovin, S., Park, S.J., Abbasi, Q.H., Alomainy, A.: An ultrathin and flexible terahertz electromagnetically induced transparency-like metasurface based on asymmetric resonators. EPJ Appl. Metamater. **10**, 4 (2023).

https://doi.org/10.1051/epjam/2023001

Padilla, W.J., et al.: Electrically resonant terahertz metamaterials: theoretical and experimental investigations. Phys. Rev. B **75**, 041102(R) (2007). https://doi.org/10.1103/PhysRevB.75.041102

Papasimakis, N., Fedotov, V.A., Zheludev, N.I., Prosvirnin, S.L.: Metamaterial analog of electromagnetically induced transparency. Phys. Rev. Lett. **101**, 253903 (2008). https://doi.org/10.1103/PhysRevLett.101.253903

Pitchappa, P., et al.: Active control of electromagnetically induced transparency analog in terahertz MEMS metamaterial. Adv. Opt. Mater. **4**, 541–547 (2016). https://doi.org/10.1002/adom.201500676

Qazilbash, M.M., et al.: Mott transition in VO_2 revealed by infrared spectroscopy and nano-imaging. Science **318**, 1750–1753 (2007).

https://doi.org/10.1126/science.1150124

Sabah, C., Dincer, F., Karaaslan, M., Unal, E., Akgol, O.: Polarization-insensitive FSS-based perfect metamaterial absorbers for GHz and THz frequencies. Radio Sci. **49**, 306–314 (2014). https://doi.org/10.1002/2013RS005340

Singh, R., Rockstuhl, C., Lederer, F., Zhang, W.: Coupling between a dark and a bright eigenmode in a terahertz metamaterial. Phys. Rev. B **79**, 085111 (2009).

https://doi.org/10.1103/PhysRevB.79.085111

Tao, H., Landy, N.I., Bingham, C.M., Zhang, X., Averitt, R.D., Padilla, W.J.: A metamaterial absorber for the terahertz regime: design, fabrication and characterization. Opt. Express **16**, 7181–7188 (2008).

https://doi.org/10.1364/OE.16.007181

Tassin, P., Zhang, L., Koschny, T., Economou, E.N., Soukoulis, C.M.: Low-loss metamaterials based on classical electromagnetically induced transparency. Phys. Rev. Lett. **102**, 053901 (2009). https://doi.org/10.1103/PhysRevLett.102.053901

Tassin, P., Zhang, L., Zhao, R., Jain, A., Koschny, T., Soukoulis, C.M.: Electromagnetically induced transparency and absorption in metamaterials: the radiating two-oscillator model and experimental confirmation. Phys. Rev. Lett. **109**, 187401 (2012). https://doi.org/10.1103/PhysRevLett.109.187401

Wang, S., Kang, L., Werner, D.H.: Hybrid resonators and highly tunable terahertz metamaterials enabled by vanadium dioxide (VO_2). Sci. Rep. **7**, 4326 (2017). https://doi.org/10.1038/s41598-017-04692-8

Yin, Z., et al.: Electrically tunable terahertz dual-band metamaterial absorber based on a liquid crystal. RSC Adv. **8**, 4197–4203 (2018).

https://doi.org/10.1039/C7RA13047C

Zhang, S., Genov, D.A., Wang, Y., Liu, M., Zhang, X.: Plasmon-induced transparency in metamaterials. Phys. Rev. Lett. **101**, 047401 (2008).

https://doi.org/10.1103/PhysRevLett.101.047401

Zylbersztejn, A., Mott, N.F.: Metal-insulator transition in vanadium dioxide. Phys. Rev. B **11**, 4383–4395 (1975). https://doi.org/10.1103/PhysRevB.11.4383